ELSEVIER

International Journal of Heat and Fluid Flow 19 (1998) 563–572

International Journal of HEAT AND FLUID FLOW

Structure of turbulent boundary layer subjected to adverse pressure gradient

Yasutaka Nagano [a,*], Toshihiro Tsuji [b], Tomoya Houra [b]

[a] *Department of Environmental Technology, Graduate School of Engineering, Nagoya Institute of Technology, Gokiso-cho, Showa-ku, Nagoya 466-8555, Japan*

[b] *Department of Mechanical Engineering, Nagoya Institute of Technology, Nagoya, Japan*

Abstract

A turbulent boundary layer subjected to a sustained adverse pressure gradient is experimentally investigated. Waveforms of fluctuating velocity components in the boundary layer, especially in the near-wall region, are remarkably elongated in time in comparison with those in zero-pressure-gradient flows, and thus time scales increase with an increasing pressure gradient parameter P^+. The increase in time scales is not in proportion to the corresponding increase in the conventional viscous time scale ν/u_τ^2. It is found that the Taylor time scale is most appropriate to describe the essential characteristics of non-equilibrium adverse pressure gradient flows. Even the near wall-limiting behavior of streamwise velocity fluctuations for different P^+ is well correlated in the coordinates based on the Taylor time scale. Moreover, in the boundary layer with an adverse pressure gradient, the contribution of sweep motions becomes equivalent to that of ejections, and outward and wallward interactions relatively increase near the wall, which evidently indicates a change in coherent structures.

Keywords: Turbulent boundary layer; Adverse pressure gradient; Scaling law; Taylor time scale; Coherent structure

Notation

C_p	wall static pressure coefficient, $C_p = (\overline{P} - \overline{P}_0)/(\rho \overline{U}_0^2/2)$
E_u, E_v	spectrum functions of velocity fluctuations u and v
$E_{\dot{u}}$	dissipation spectrum of velocity fluctuations u
f	frequency
f'	dimensionless frequency, $f' = f\nu/\overline{U}_0^2$
f''	dimensionless frequency, $f'' = f\tau_E$
k	turbulent kinetic energy
$\overline{P}$	mean pressure
P^+	dimensionless pressure gradient parameter, $P^+ = \nu(\mathrm{d}\overline{P}/\mathrm{d}x)/\rho u_\tau^3$
$\overline{P}_0$	reference inlet pressure
R_θ	Reynolds number based on momentum thickness, $R_\theta = \overline{U}_e\theta/\nu$
$R_u(t)$	auto-correlation coefficient of u
T_E	Eulerian integral time scale, $T_\mathrm{E} = \int_0^\infty R_u(t)\,\mathrm{d}t$
t	time
$\overline{U}$	mean velocity in x direction
$\overline{U}_e$	free-stream velocity
$\overline{U}_0$	reference inlet velocity
u, v, w	fluctuating velocity components in x, y and z directions
u_τ	friction velocity, $u_\tau = \sqrt{\tau_\mathrm{w}/\rho}$
W_m	weighted p.d.f. of moment m
x, y, z	streamwise, wall-normal and spanwise coordinates
y^+	dimensionless distance from wall, $y^+ = u_\tau y/\nu$

Greek

β	Clauser pressure gradient parameter, $\beta = (\delta^*/\tau_\mathrm{w})\,\mathrm{d}\overline{P}/\mathrm{d}x$
γ	intermittency factor
δ_{99}	boundary layer thickness
δ^*, θ	displacement and momentum thicknesses
ε	dissipation rate of k
ν	kinematic viscosity
ρ	density
τ_B	mean burst period
τ_E	Taylor time scale or Eulerian dissipation time scale, $\tau_\mathrm{E} = \sqrt{2\overline{u^2}/\overline{(\partial u/\partial t)^2}}$
$\tau_{\mathrm{E}s}$	Taylor time scale in linear (viscous) sublayer
τ_m	time scale corresponding to mean shear rate, $\tau_\mathrm{m} = 1/(\partial\overline{U}/\partial y)$
τ_w	wall shear stress

Subscript and superscripts

0	reference inlet point
$(\hat{\ })$	normalization by r.m.s. value
$\overline{(\ )}$	time mean value
$(\ )^+$	normalization by inner variables (u_τ, ν)

* Corresponding author. E-mail: nagano@heat.mech.nitech.ac.jp.

0142-727X/98/$ – see front matter
PII: S0142-727X(98)10013-9

1. Introduction

In theory as well as in practice, it is of fundamental importance to investigate the effects of pressure gradients on the structure of turbulent boundary layers. From our previous experiment on an adverse-pressure-gradient (APG) turbulent boundary layer (Nagano et al., 1992), we have obtained the following results: (1) the standard log-law velocity profile for a zero-pressure-gradient (ZPG) boundary layer does not hold in APG turbulent boundary layers; (2) near-wall distributions of r.m.s. velocity fluctuations cannot scale with the wall parameters, u_τ and ν; and (3) the response time of turbulence to the imposed APG, which relates closely to the redistribution process of turbulent kinetic energy, differs among streamwise, wall-normal and spanwise velocity components.

Although the viscous wall unit is a standard parameter for scaling the equilibrium turbulent boundary layers (Skåre and Krogstad, 1994), the above fact implies that another characteristic time scale or length scale must be introduced in order to scale the non-equilibrium APG flows. Thus, the main objectives of the present study are: (i) to reveal the in-depth turbulent structure inherent in the APG flows; (ii) to find an appropriate time scale which provides universal scaling of the near-wall turbulent statistics; (iii) to understand the physical meanings and roles of the time scale in characterizing the APG flows; and (iv) to find structures, if any, which cannot be described in terms of the time scale.

2. Experimental apparatus

We used the same experimental apparatus as in Nagano et al. (1992). Working fluid is air. The test section is composed of a flat-plate on which a turbulent boundary layer develops, and a roof-plate to adjust pressure gradients. The aspect ratio at the inlet to the test section is 13.8:1. Under the present measurement conditions, the free-stream turbulence level is below 0.15% and velocity non-uniformities in the y-(normal to the wall) and z-(lateral) directions are within 0.17% and 0.63%, respectively. Therefore, nearly ideal, two-dimensional uniform inflow is obtained. To generate a stable and fully-developed turbulent boundary layer, a row of equilateral triangle plates is located at the inlet to the test section as a tripping device. It is confirmed that even at the end of the test section the velocity profile in the boundary layer on the pressure-adjusting roof-plate becomes close to the Blasius' laminar-flow solution and this quasi-laminar boundary layer is separated by the uniform free-stream from the objective turbulent boundary layer developing on the flat-plate. Thus, there are no interactions between the two.

Velocity measurement was done with hot-wire probes, i.e., a handmade subminiature (Ligrani and Bradshaw, 1987) normal hot-wire (dia.: 3.1 μm; length: 0.6 mm), and two types of specially devised X-probes (dia.: 3.1 μm; length: 0.6 mm $\simeq$ 7.5 ν/u_τ; wire spacing: 0.30 mm $\simeq$ 3.8 ν/u_τ for measurement of u and v, and wire spacing: 0.23 mm $\simeq$ 2.9 ν/u_τ for u and w). To convert the hot-wire outputs into the velocity components, we used the look-up-table method (Lueptow et al., 1988). Also, the inevitable bias error, which is ascribed to the finite separation of the wires in using an X-probe, was removed in accordance with the procedure indicated by Tagawa et al. (1992). As a result, the measured velocity fluctuations near the wall in the ZPG flow show good agreement with the DNS data (Spalart, 1988) of the ZPG flow (see Nagano et al., 1992).

The important flow parameters are listed in Table 1.

In the present APG flow, the pressure gradient dC_p/dx keeps a nearly constant value of 0.6 m^{-1} over 65 mm $\leqslant x \leqslant$ 700 mm and then decreases slowly. On the other hand, the pressure gradient parameter normalized by inner variables P^+ and the Clauser parameter β increase monotonously, thus yielding moderate to strong adverse pressure gradients.

Table 1
Flow parameters ($\overline{U}_0 = 10.8$ m/s)

x mm	$\overline{U}_e$ m/s	δ_{99} mm	u_τ m/s	R_θ	P^+	β
525	10.8	13.3	0.481	1070	0	0
925	10.8	19.9	0.465	1620	0	0
523	9.08	16.2	0.390	1290	9.12×10^{-3}	0.77
723	8.18	24.6	0.307	1880	1.93×10^{-2}	2.19
925	7.54	34.2	0.251	2660	2.56×10^{-2}	3.95
1121	6.68	46.1	0.197	3350	2.87×10^{-2}	5.32

The friction velocities in the APG flows are determined with the method of Nagano et al. (1992). In the vicinity of the wall, the apparent velocities $\overline{U}_m^+$ measured with hot wires deviate systematically from the linear profiles, $\overline{U}^+ = y^+$, as the wall is approached. This can be ascribed to the wall proximity effect of hot-wire outputs. Previous extensive studies investigating this wall proximity effect (for example, Oka and Kostic, 1972; Hebbar and Melnik, 1978; Bhatia et al., 1982; Janke, 1987; Chew et al., 1995) have confirmed experimentally and numerically that once material of a wall, the geometrical factors of a hot-wire, and the operating overheat-ratio are given, the amount of this deviation can be determined universally, independent of values of wall shear stress, so that $\overline{U}_m^+ = f(y^+)$. As seen in Fig. 1, the apparent velocities $\overline{U}_m^+$ in the present experiments collapse very well onto a unique curve $f(y^+)$, being consistent with the previous findings. We utilize this relationship to determine the friction velocities u_τ as follows. First, we determine the friction velocities by using the established Clauser method (Clauser, 1954) in the ZPG flows, where the existence of the log-law has been definitely confirmed, and determine the near-wall relationship $\overline{U}_m^+ = f(y^+)$. Then, in APG flows, we use this relationship in reverse as a calibration curve to determine the friction velocities u_τ.

3. Statistical characteristics

3.1. Mean velocity and turbulent intensities

Fig. 2 shows the mean velocity profiles normalized by the friction velocity u_τ. As clearly seen from this figure, the velocity

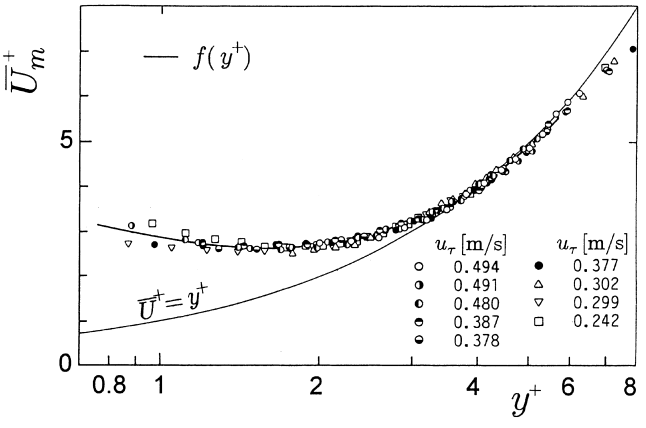

Fig. 1. Near-wall distributions of apparent velocities $\overline{U}_m^+$ in various zero-pressure-gradient flows.

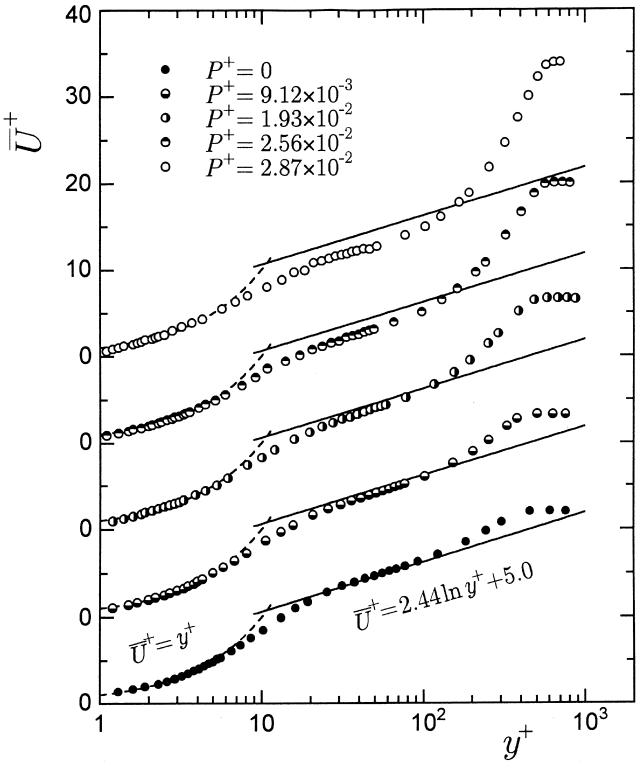

Fig. 2. Mean velocity profiles in wall coordinates in adverse-pressure-gradient flows. The solid lines denote the standard log-law ($\overline{U}^+ = 2.44 \ln y^+ + 5.0$), and the broken lines the linear profiles ($\overline{U}^+ = y^+$).

profiles in APG flows lie below the following 'standard' log-law profile for ZPG flows:

$$\overline{U}^+ = 2.44 \ln y^+ + 5.0. \quad (1)$$

This important characteristic of the APG flows conforms to our previous result (Nagano et al., 1992), and is also confirmed by the direct numerical simulation (DNS) of Spalart and Watmuff (1993) and by the recent measurement of Debisschop and Nieuwstadt (1996). Moreover, this finding is corroborated by the recent DNS for an APG recovery region of backward-facing step flow (Le et al., 1997).

The intensity profiles of fluctuating velocity components u, v and w, normalized by the free-stream velocity $\overline{U}_0$ at the inlet to the test section are presented in Fig. 3. The abscissa is the distance from the wall normalized with the boundary layer thickness δ_{99}. With an increasing APG effect, the reduction in turbulence intensities can be seen in the wall region ($y/\delta_{99} < 0.4$), whereas all the profiles in the outer layer are kept unchanged. Thus, turbulence intensities are considered to be unchanged along streamlines of the mean flow lying outside the wall region, since the streamlines and the lines of constant y/δ_{99} are approximately the same. The APG changes the intensities of velocity fluctuations near the wall in the order of streamwise (u), spanwise (w), and wall-normal (v) components. These profiles cannot be correlated in conventional wall coordinates even in the near-wall region. As shown in Fig. 4, the distributions of $\sqrt{\overline{u^2}}/u_\tau$ near the wall follow each P^+-dependent straight line which coincides with the origin. The same tendency is also confirmed from the DNS (Spalart and Watmuff, 1993). This means that the viscous wall unit cannot be used to describe the unique features of the present and DNS's APG flows.

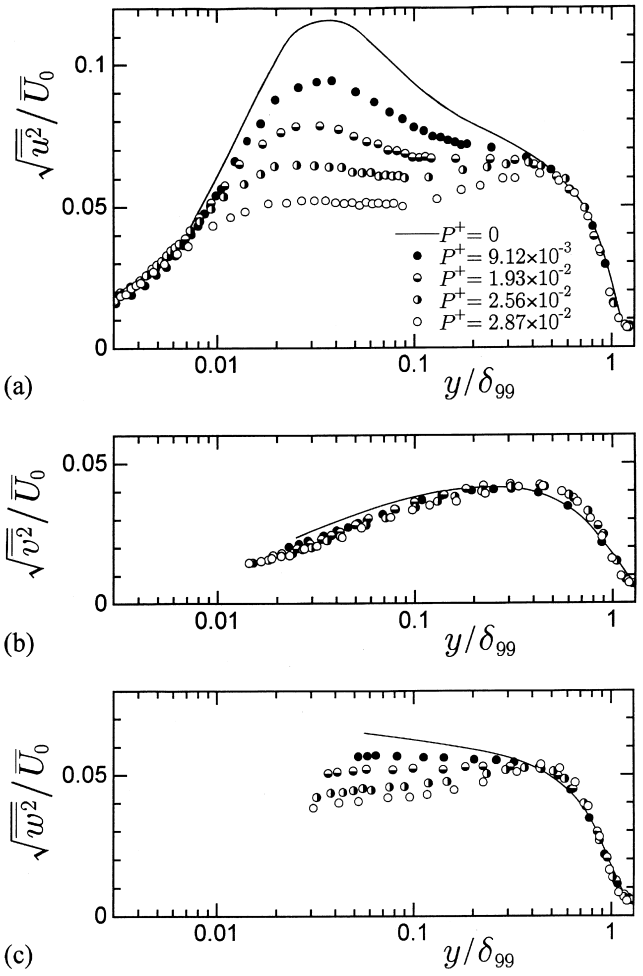

Fig. 3. Turbulence intensities of fluctuating velocity components: (a) streamwise; (b) wall-normal; (c) spanwise.

To understand the basic mechanism of the above feature of APG flows, we have investigated the characteristics of instantaneous signal traces of the fluctuating velocity components u and v together with the Reynolds shear stress uv. The results in the near-wall region and those at the outer edge of

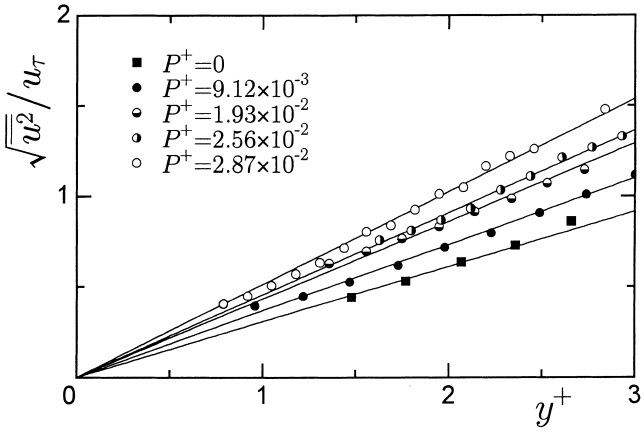

Fig. 4. Wall-limiting behavior of $\sqrt{\overline{u^2}}/u_\tau$.

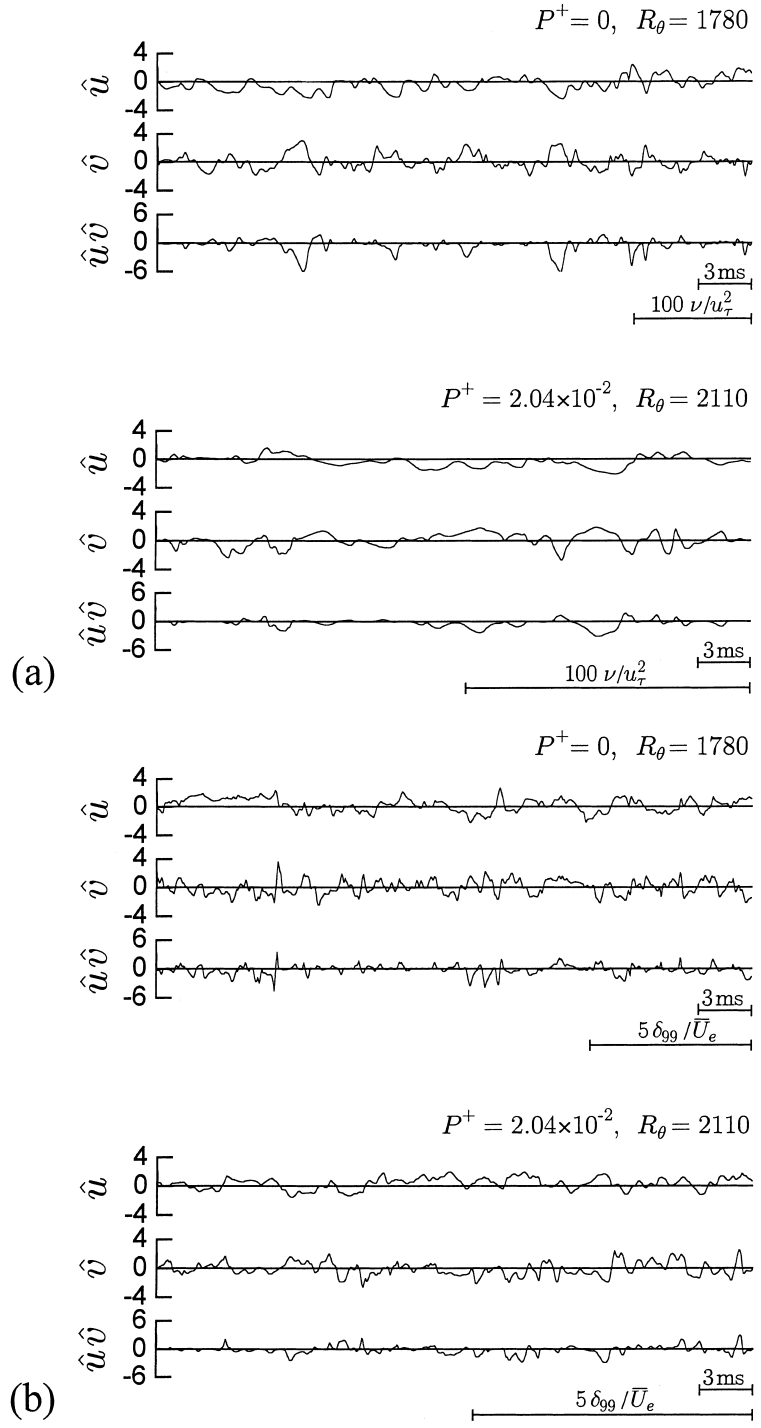

Fig. 5. Signal traces of $\hat{u}$, $\hat{v}$ and $\hat{u}\hat{v}$: (a) inner layer ($y^+ \simeq 18$, $y/\delta_{99} \simeq 0.03$); (b) outer layer ($y^+ \simeq 260$, $y/\delta_{99} \simeq 0.5$).

the log-law region are shown in Fig. 5(a) and (b), respectively, in comparison with the ZPG flow. A circumflex denotes the normalization by the respective r.m.s. value. It is quite clear from Fig. 5(a) that, despite having nearly the same R_θ value, the time scales of velocity fluctuations in the wall region of the APG flow are extremely elongated and become different from those in the ZPG flow; that is, turbulent motions of the APG flow become gentle and less active, which may correspond to the observed low production of turbulence energy (Nagano et al., 1992). In the outer region, on the other hand, there is a small (but not negligible) difference in the instantaneous signal traces between the ZPG and APG flows.

3.2. Spectra

Power spectra of u and v fluctuations in the log region ($y^+ \simeq 50$) are presented in Fig. 6(a) and (b), respectively, against the dimensionless frequency $f' = f\nu/\overline{U}_0^2$. As expected from the waveforms in Fig. 5, the frequencies of energy-containing eddies in both spectra gradually shift toward the lower

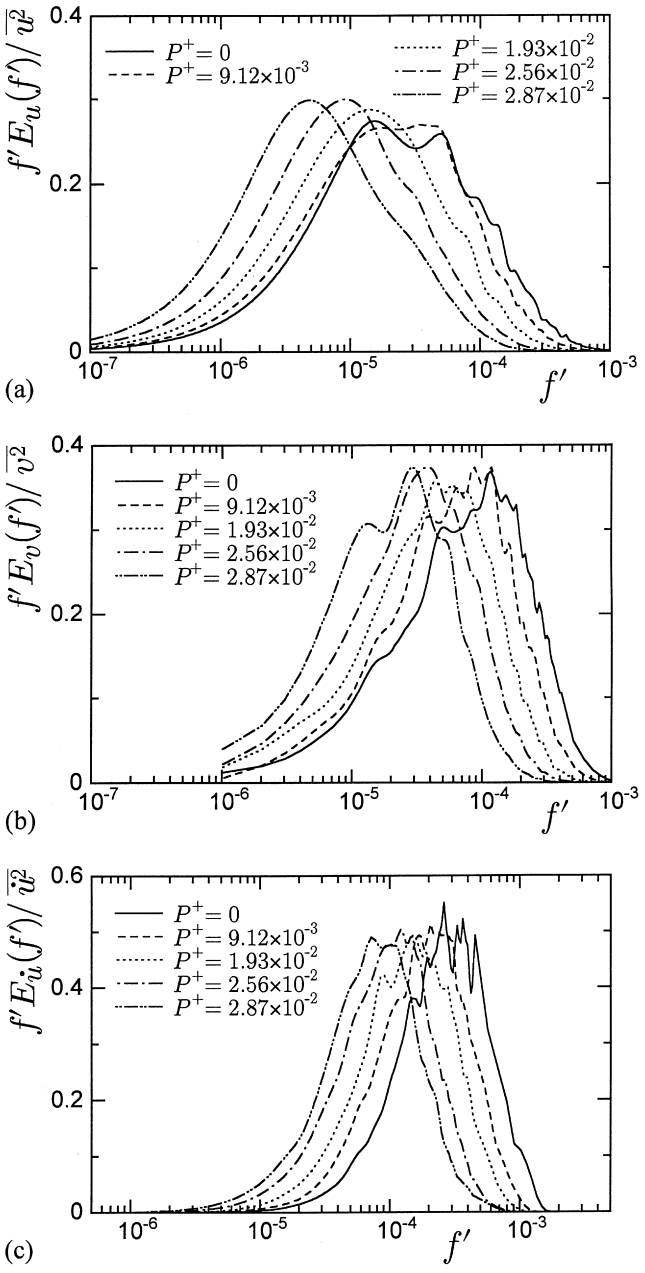

Fig. 6. Power spectra of velocity fluctuation in the log region ($y^+ \simeq 50, y/\delta_{99} \simeq 0.1$): (a) streamwise fluctuation u; (b) wall-normal fluctuation v. (c) Spectra of $(\partial u/\partial t)^2$.

frequency with increasing P^+. To clarify the APG effect on velocity fluctuations at high frequencies, we have examined the spectra of $(\partial u/\partial t)^2$, which may be considered an approximation of the dissipation, and present them in Fig. 6(c). The spectra of $(\partial u/\partial t)^2$ also shift toward the lower frequency as P^+ increases. Such changes in power and dissipation spectra are observed in both the near-wall and outer regions.

3.3. Scaling law

The above facts indicate that an adverse pressure gradient has a strong influence on turbulence statistics selectively in the near-wall region, and that it is the time scale that represents the essential characteristics of APG turbulent boundary layers. Thus, we proceed to investigate the flow structures from the viewpoint of the temporal behavior of turbulence quantities so as to obtain an appropriate time scale which provides a universal scaling law for the near-wall turbulence statistics of APG flows.

In the present study, we have examined the turbulence structures of the APG flow using the following six distinct characteristic time scales (see Notation for definition):

viscous time scale:	ν/u_τ^2
Kolmogorov time scale:	$\sqrt{\nu/\varepsilon}$
Taylor time scale:	τ_E
time scale for energy-containing eddies:	k/ε
integral time scale:	T_E
time scale corresponding to mean shear rate:	τ_m

where k and ε are the turbulent kinetic energy and its dissipation rate, respectively. Note that the viscous time scale ν/u_τ^2 is uniquely determined at a given x location, while the other parameters vary locally in the y direction.

By using the above six time scales, we have analyzed the temporal turbulent structures of the APG flows. As a result, the Taylor time scale τ_E is found to be the most appropriate for representing the temporal behavior of turbulence quantities and for universally scaling the turbulence statistics. Generally, in high-Reynolds number flows, the Taylor time scale τ_E and the viscous dissipation ε are related to each other through the expression $\varepsilon = 30\nu\overline{u^2}/(\overline{U}^2\tau_E^2)$.

The sample results of scaling raw waveforms in Fig. 5 with τ_E are presented in Fig. 7. The corresponding various spectra in the log region ($y^+ \simeq 50$) arranged with a new dimensionless frequency, $f'' = f\tau_E$, are presented in Fig. 8. As can be clearly seen from these figures, we conclude that the Taylor time scale is the best scaling parameter for both ZPG and APG flows.

The distributions of the measured Taylor time scale τ_E in the y direction are shown in Fig. 9. One may find that τ_E increases with increasing pressure gradient parameters P^+. In proximity to the wall, however, τ_E becomes almost constant for a given P^+. In what follows, we apply the characteristic time scale τ_E to scaling various turbulence statistics.

First, we present the scaling of the wall-limiting behavior of streamwise turbulence intensity $\sqrt{\overline{u^2}}$ in Fig. 10. Here, τ_{Es} defined by a value of τ_E at the outer edge of the viscous sublayer, i.e., $y^+ = 3$, is adopted, and the coordinate y is normalized with the characteristic length scale $u_\tau\tau_{Es}$. If the viscous wall unit is used as a length scale, there appear remarkable differences in the wall-limiting behavior between the ZPG and APG flows with a systematic deviation from the ZPG case as depicted in Fig. 4. On the other hand, the use of the time scale τ_{Es} makes all the profiles collapse irrespective of the values of P^+ as shown in Fig. 10.

Next, from the waveforms stretched in accordance with the Taylor time scale τ_E in APG flows, we have obtained intermittency factors γ by using the method of Hedley and Keffer (1974). As shown in Fig. 11, the distributions of intermittency factors in APG flows become identical to those in the ZPG flow (The curve in Fig. 11 is the Gaussian error function, whose average position of the interface between turbulent and non-turbulent fluid is $0.9\delta_{99}$, and r.m.s. value of the difference between the instantaneous and average positions of the interface is $0.14\delta_{99}$.)

These results suggest that if we make a proper choice of a scaling parameter based on the knowledge of turbulence structures, we may describe the features of adverse pressure gradient flows uniquely even under non-equilibrium conditions.

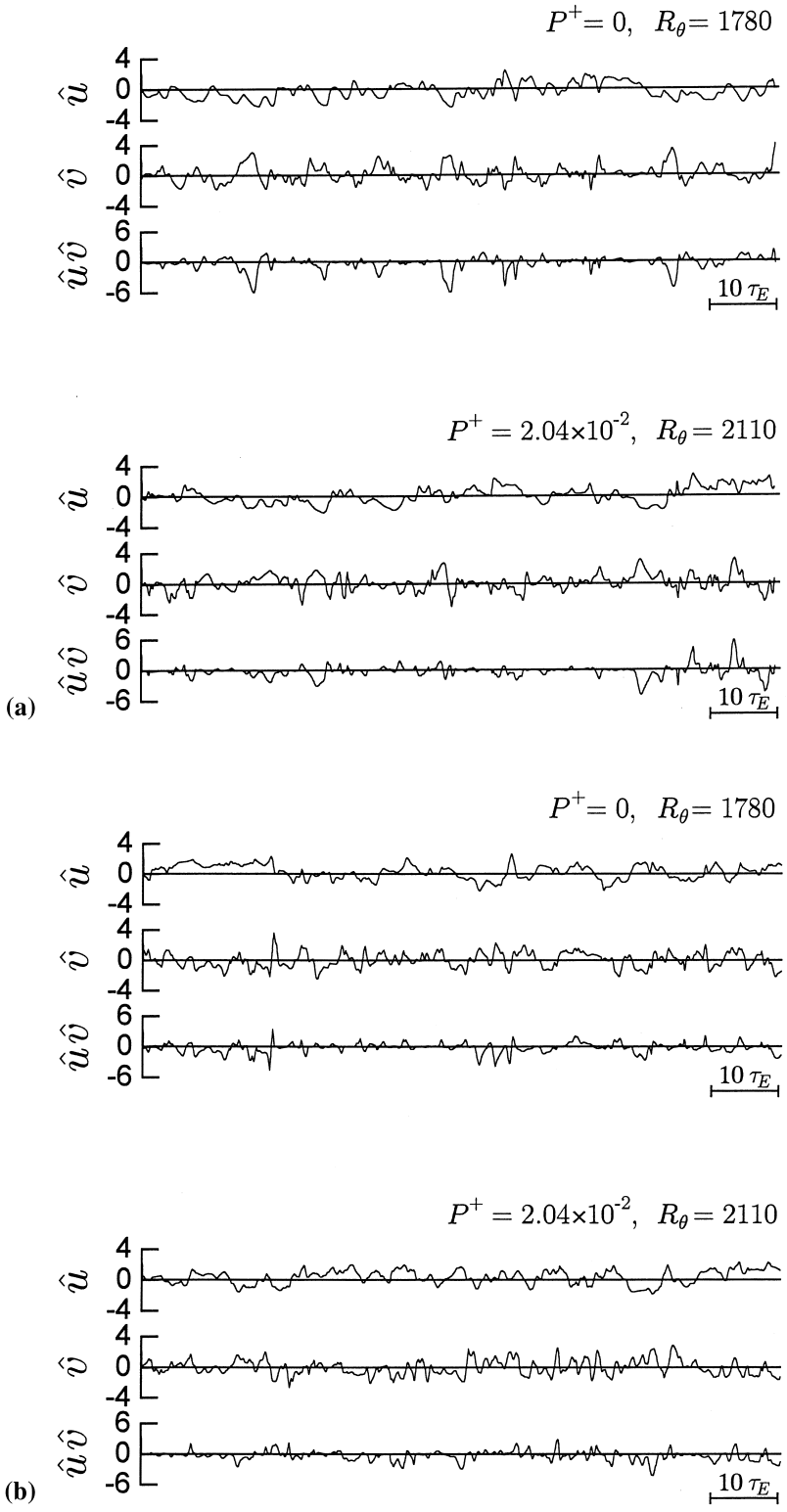

Fig. 7. Signal traces of $\hat{u}$, $\hat{v}$ and $\hat{u}\hat{v}$ normalized by Taylor time scale τ_E: (a) inner layer ($y^+ \simeq 18, y/\delta_{99} \simeq 0.03$); (b) outer layer ($y^+ \simeq 260, y/\delta_{99} \simeq 0.5$).

4. Dynamical characteristics

To identify any scale-irrelevant structures hidden in a flow, we now investigate the dynamical features of APG flows. We first investigate the relation between τ_E and the characteristic time scale pertaining to the bursting phenomena, τ_B, obtained from the short-time averaged auto-correlation function method (Kim et al., 1971; Hishida and Nagano, 1979). There are many arguments about the scaling of mean burst period in APG flows (e.g., White and Tiederman, 1990; Tillman and

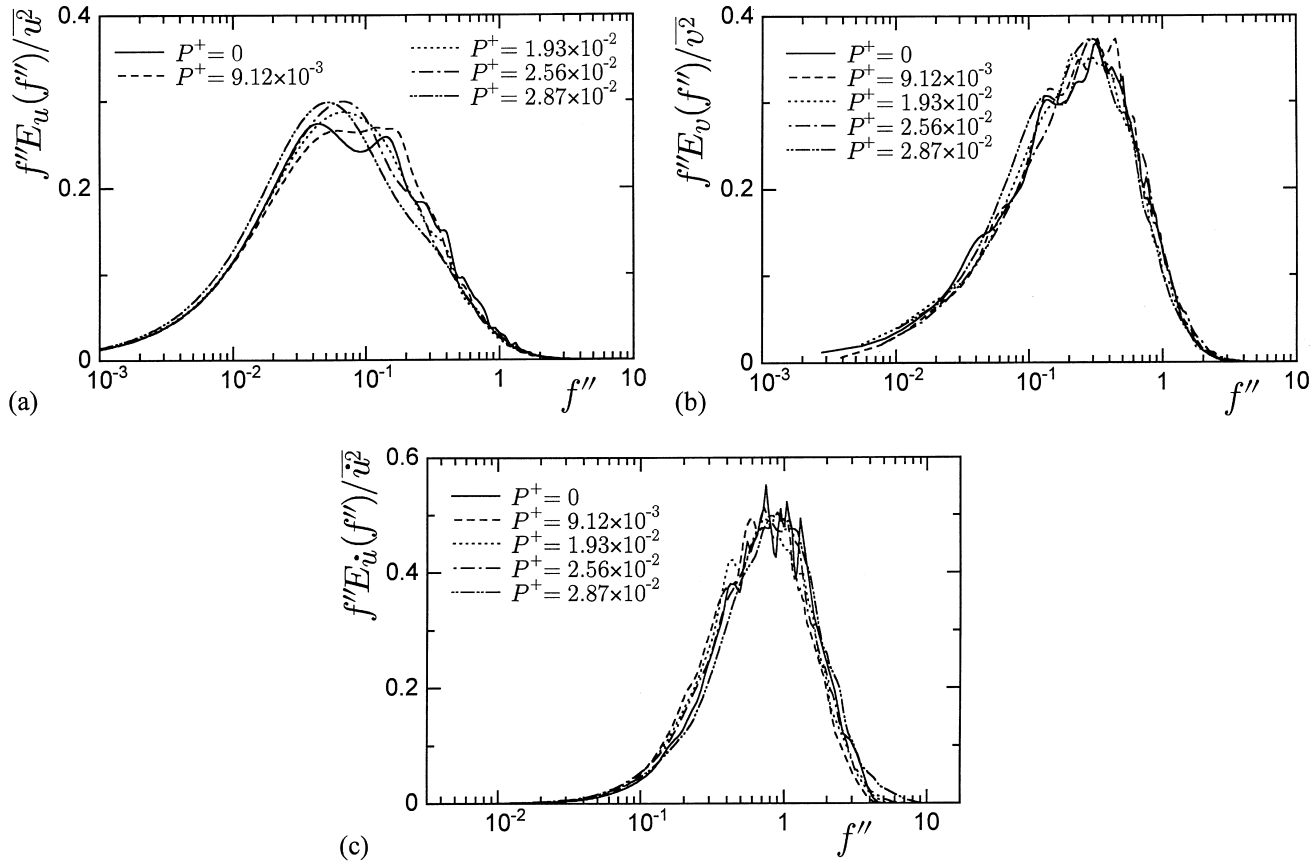

Fig. 8. Power spectra of velocity fluctuation arranged with dimensionless frequency f'' in the log region ($y^+ \simeq 50, y/\delta_{99} \simeq 0.1$): (a) streamwise fluctuation u; (b) wall-normal fluctuation v. (c) Spectra of $(\partial u/\partial t)^2$.

Kistler, 1996). Bandyopadhyay (1982) mentioned that a universal value of the non-dimensional period between bursting does not exist, though it might be an extreme case. It becomes obvious from Fig. 12 that the mean burst period τ_B changes strikingly with P^+. However, as shown in Fig. 13, the normalized period τ_B/τ_{Es} tends to collapse for any pressure gradient level. This means that τ_E closely relates to the dynamical coherent structure. It should be noted that the Taylor time scale τ_E is also appropriate to scale mean burst period in a favorable pressure gradient flow (Misu et al., 1992), and to scale the event durations of spanwise vorticity fluctuation in ZPG flows (Klewicki and Falco, 1996).

The coherent structure of turbulence may affect statistical values, especially higher order moments (Nagano and Tagawa, 1988). Thus, we have examined the fractional contributions (Wallace et al., 1972) to Reynolds shear stress $-\overline{uv}$. Fig. 14 shows the results obtained for ZPG and APG flows. In the log

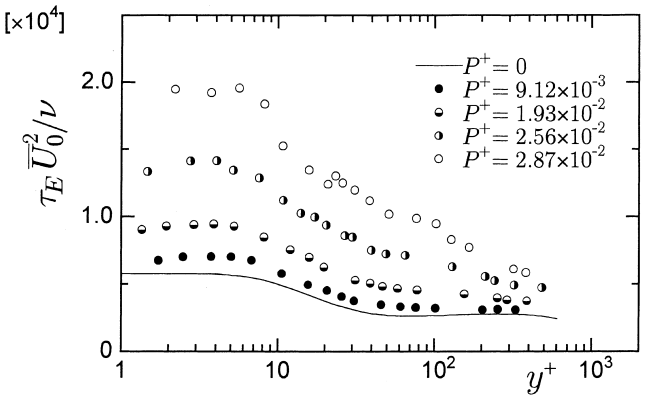

Fig. 9. Distributions of Taylor time scale τ_E.

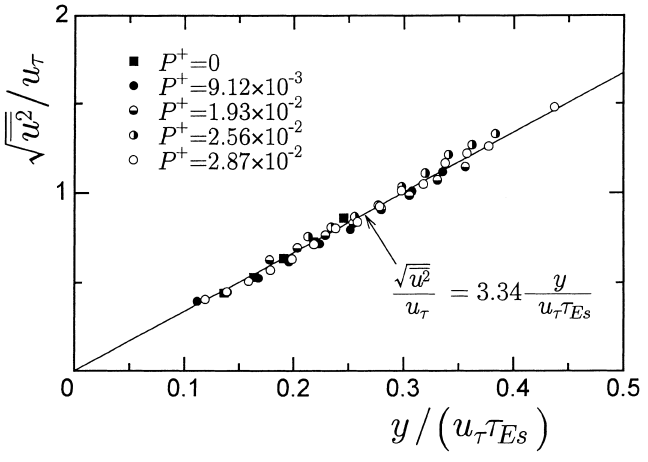

Fig. 10. Scaling of wall-limiting behavior of streamwise intensity $\sqrt{\overline{u^2}}$ with Taylor time scale τ_{Es}.

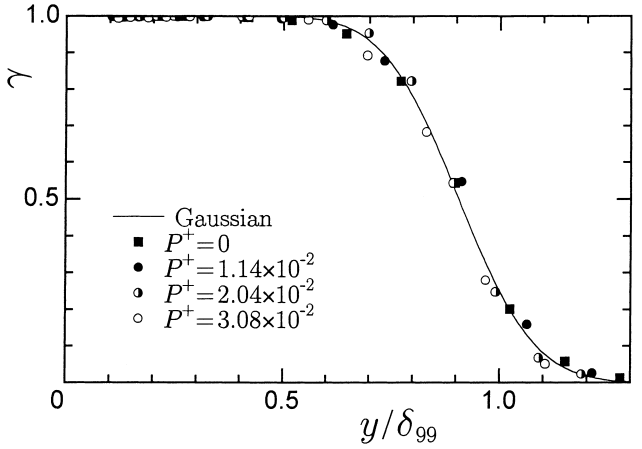

Fig. 11. Intermittency factors γ in APG flow.

region of the ZPG flow, the most contributive motion is the ejection (Q2), with the sweep motion (Q4) following it. The contributions of interactions (Q1, Q3) are fairly small in comparison with those of the active motions (Q2, Q4). Such behavior is also observed in a pipe flow (Nagano and Tagawa, 1988), and is considered to be a characteristic of the canonical wall flow.

On the other hand, in the APG flow, the situation is remarkably different from that in the ZPG flow. The contributions of ejection and sweep motions (Q2, Q4) become equivalent and increase toward the wall. Correspondingly, the negative contributions of interactions (Q1, Q3) increase near the wall. This fact indicates that in APG flows energy transfer through the turbulent diffusion toward the wall becomes dominant, and that a relative increase in inactive motions (Q1, Q3) results (Bradshaw, 1967).

To understand in detail the quantitative contributions of each classified fluid motion to the Reynolds shear stress $-\overline{uv}$, we introduce the weighted p.d.f. of $-\hat{u}\hat{v}$, $W_{-\hat{u}\hat{v}}(\hat{u},\hat{v})$, defined by

$$W_{-\hat{u}\hat{v}}(\hat{u},\hat{v}) = -\hat{u}\hat{v}P(\hat{u},\hat{v}), \tag{2}$$

where $P(\hat{u},\hat{v})$ is the joint p.d.f. for u and v fluctuations (Nagano and Tagawa, 1988). The typical results in the log region ($y^+ \simeq 50$) are shown in Fig. 15. The solid and broken contour lines denote the positive and negative values, respectively. The integrated volume of the weighted p.d.f. in each quadrant corresponds to the respective contribution to the Reynolds shear stress. In the APG flow, the contribution of sweep motions becomes larger than that of ejections in the log region.

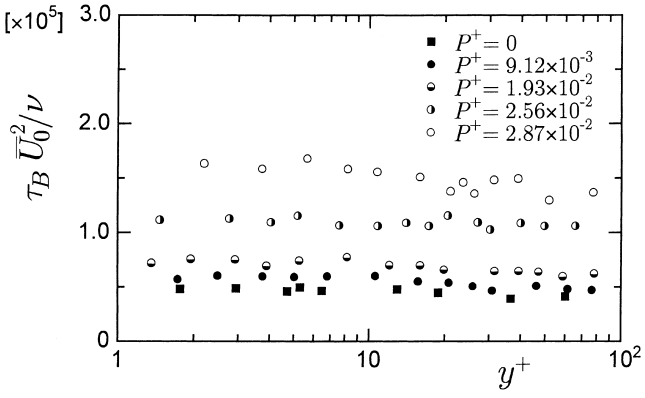

Fig. 12. Mean period of intermittent bursts.

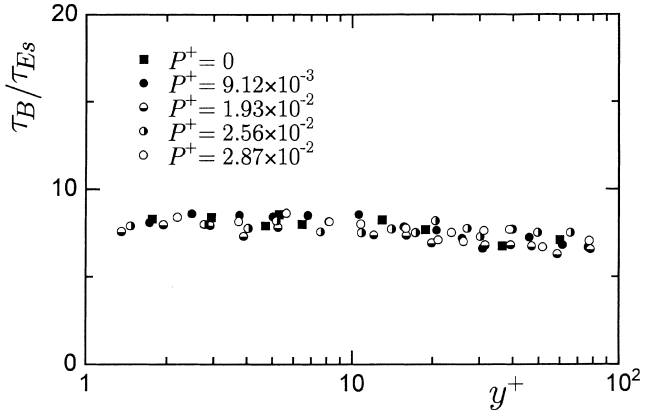

Fig. 13. Mean period of intermittent bursts normalized by τ_{Es}.

Furthermore, the corresponding distributions of the p.d.f. differ between ejections and sweeps, which indicates changes in the coherent structure between the ZPG and APG flows. Note that these changes in the coherent structure cannot be identified only with a change in the time scale.

5. Conclusions

Experimental investigation has been made on non-equilibrium turbulent boundary layers subjected to adverse pressure gradients. The results can be summarized as follows:

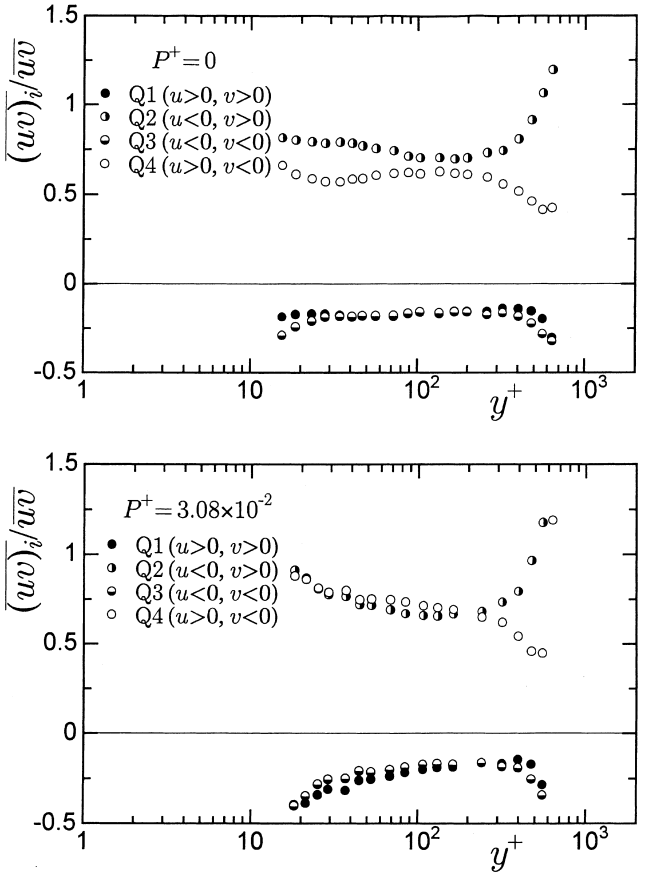

Fig. 14. Fractional contributions to Reynolds shear stress.

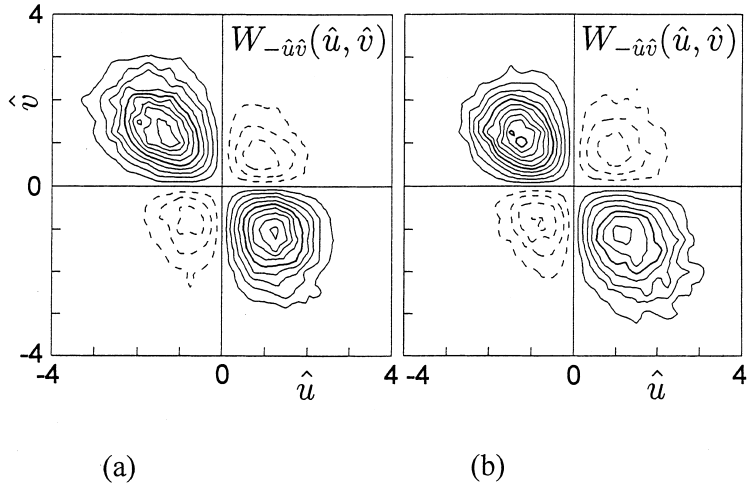

Fig. 15. Weighted p.d.f.s of $-\hat{u}\hat{v}$ in the log region ($y^+ \simeq 50, y/\delta_{99} \simeq 0.1$). The interval between the contour lines is 0.01; (a) $P^+ = 0$; (b) $P^+ = 3.08 \times 10^{-2}$.

(1) In the APG flow, the characteristic time scale of the flow is exceedingly elongated in the near-wall region, in comparison with the ZPG flow at nearly the same R_θ. This difference should be related closely to the progressive decrease in turbulence intensities in the near-wall region, and can be ascribed to the retardation of turbulence production.
(2) In the outer region, there is a slight difference in the instantaneous velocity signals and in the distributions of turbulence intensities between the ZPG and APG flows.
(3) The Taylor time scale τ_E is the most appropriate to describe the essential characteristics of the near-wall structure of non-equilibrium APG flows.
(4) The conventional scaling law using the viscous time scale ν/u_τ^2 cannot be applied to the scaling of the near-wall statistics of the non-equilibrium APG flows. Instead of ν/u_τ^2, the Taylor scale τ_E in the near-wall region, combined with u_τ, may provide the best scaling law.
(5) In APG flows, the contribution of sweep motions becomes equivalent to that of ejections, and outward and wallward interactions relatively increase near the wall, which evidently indicates a change in coherent structures.

References

Bandyopadhyay, P.R., 1982. Period between bursting in turbulent boundary layers. Phys. Fluids 25, 1751–1754.

Bhatia, J.C., Durst, F., Jovanovic, J., 1982. Corrections of hot-wire anemometer measurements near walls. J. Fluid Mech. 122, 411–431.

Bradshaw, P., 1967. The turbulence structure of equilibrium boundary layers. J. Fluid Mech. 29, 625–645.

Chew, Y.T., Shi, S.X., Khoo, B.C., 1995. On the numerical near-wall corrections of single hot-wire measurements. Int. J. Heat Fluid Flow 16, 471–476.

Clauser, F.H., 1954. Turbulent boundary layers in adverse pressure gradients. J. Aero. Sci. 21, 91–108.

Debisschop, J.R., Nieuwstadt, F.T.M., 1996. Turbulent boundary layer in an adverse pressure gradient: effectiveness of riblets. AIAA J. 34, 932–937.

Hebbar, K.S., Melnik, W.L., 1978. Wall region of a relaxing three-dimensional incompressible turbulent boundary layer. J. Fluid Mech. 85, 33–56.

Hedley, T.B., Keffer, J.F., 1974. Turbulent/non-turbulent decisions in an intermittent flow. J. Fluid Mech. 64, 625–644.

Hishida, M., Nagano, Y., 1979. Structure of turbulent velocity and temperature fluctuations in fully developed pipe flow. Trans. ASME, J. Heat Transfer 101, 15–22.

Janke, G., 1987. Hot wire in wall proximity. In: Comte-Bellot, G., Mathieu, J. (Eds.), Advances in Turbulence, Springer, Berlin, pp. 488–498.

Kim, H.T., Kline, S.J., Reynolds, W.C., 1971. The production of turbulence near a smooth wall in a turbulent boundary layer. J. Fluid Mech. 50, 133–160.

Klewicki, J.C., Falco, R.E., 1996. Spanwise vorticity structure in turbulent boundary layers. Int. J. Heat Fluid Flow 17, 363–376.

Le, H., Moin, P., Kim, J., 1997. Direct numerical simulation of turbulent flow over a backward-facing step. J. Fluid Mech. 330, 349–374.

Ligrani, P.M., Bradshaw, P., 1987. Subminiature hot-wire sensors: development and use. J. Phys. E: Sci. Instrum. 20, 323–332.

Lueptow, R.M., Breuer, K.S., Haritonidis, J.H., 1988. Computer-aided calibration of X-probes using a look-up table. Exp. Fluids 6, 115–118.

Misu, I., Saida, N., Furukawa, Y., 1992. Average time between bursts in a favorable pressure gradient. Trans. JSME B 58, 556, 3590–3595.

Nagano, Y., Tagawa, M., 1988. Statistical characteristics of wall turbulence with a passive scalar. J. Fluid Mech. 196, 157–185.

Nagano, Y., Tagawa, M., Tsuji, T., 1992. Effects of adverse pressure gradients on mean flows and turbulence statistics in a boundary layer. In: Durst, F., Friedrich, R., Launder, B.E., Schmidt, F.W., Schumann, U., Whitelaw, J.H. (Eds.), Turbulent Shear Flows 8, Springer, Berlin, pp. 7–21.

Oka, S., Kostic, Z., 1972. Influence of wall proximity on hot-wire velocity measurements. DISA Information 13, 29–33.

Skåre, P.E., Krogstad, P.-, Å.1994. A turbulent equilibrium boundary layer near separation. J. Fluid Mech. 272, 319–348.

Spalart, P.R., 1988. Direct simulation of a turbulent boundary layer up to $R_\theta = 1410$. J. Fluid Mech. 187, 61–98.

Spalart, P.R., Watmuff, J.H., 1993. Experimental and numerical study of a turbulent boundary layer with pressure gradients. J. Fluid Mech. 249, 337–371.

Tagawa, M., Tsuji, T., Nagano, Y., 1992. Evaluation of X-probe response to wire separation for wall turbulence measurements. Exp. Fluids 12, 413–421.

Tillman, T.G., Kistler, A.L., 1996. Scaling of the bursting frequency for turbulent boundary layers approaching separation. AIAA J. 34, 1070–1072.

Wallace, J.M., Eckelmann, H., Brodkey, R.S., 1972. The wall region in turbulent shear flow. J. Fluid Mech. 54, 39–48.

White, J.B., Tiederman, W.G., 1990. The effect of adverse pressure gradient on turbulent burst structure in low-Reynolds number equilibrium boundary layers. ONR Rept. PME-FM-90-2.